KSME International Journal, Vol. 16 No. 6, pp. 745~756, 2002

Reference Trajectory Analysis and Trajectory Control by Bank Angle for Re-Entry Vehicle

Dae Woo Lee, Kyeum Rae Cho*

Department of Aerospace Engineering, Pusan National University, Pusan 609-735, Korea

The re-entry problem consists of guidance design and trajectory control. This paper summarizes the detailed relationships between the velocity, drag acceleration and altitude in determining reference trajectories. The computational issues are also addressed, and the performance of the proposed simple nonlinear control of a bank angle for the longitudinal/lateral trajectory is demonstrated. In particular, the fixed bank angle methods that can reduce the drag acceleration errors at low-speeds are proposed. The importance of bank reversals with respect to the azimuth errors is also elucidated.

Key Words: Re-Entry, Reference Trajectory, Control and Guidance, Fixed Bank Angle Methods

1. Introduction

The International Space Station (ISS) is scheduled to replace the space station Mir. Since June 1998 the ISS has been under construction at the height of 435km above the earth by a joint effort between the USA, Russia, Japan, Canada and several European countries. The ISS consists of the base structure and many laboratories. Considering a round-trip transportation of freight and crew members, important stages of the space flight profile are the launch of the space vehicle, orbit entry, rendezvous with the space station, separation from the space station, de-orbit, re-entry into the atmosphere, TAEM(Terminal Area Energy Management), and finally, approaching and landing at the runway. Among these, guidance and control of the atmospheric re-entry phase can be represented as the flight onto the reference trajectory, which has to satisfy many constraint conditions and execute stable flight.

* Corresponding Author,
E-mail : krcho@pusan.ac.kr
TEL : +82-51-510-2309; **FAX** : +82-51-513-3760
Department of Aerospace Engineering, Pusan National University, Pusan 609-735, Korea. (Manuscript **Received** March 31, 2000; **Revised** February 14, 2002)

From the very beginning in the design of the space shuttle in the USA, the guidance and control system for re-entry vehicle has been developed. The Space Shuttle has a high load capacity and can decelerate efficiently by gliding like a plane, but it requires expensive maintenance. For these reasons, a new generation of reusable payload vehicles have been developed in several countries. RLV of the USA and Hope-X of Japan are the typical examples. RLV has been developed from a series of experimental vehicles denoted X-33. Hope-X is based on the experimental vehicles named Orex, Alflex, and Hyflex. In the development of these reusable space vehicles, guidance and control for atmospheric re-entry has become an important issue.

There are many researchers who have worked on the re-entry problem. In 1983, Harpold and Gavert (1979) analyzed the reference trajectory by dividing it into distinct phases depending on the dominant constraints at each phase. Although they presented the characteristics of range prediction as well as the parameters of reference trajectory at each phase, the relationships between the drag acceleration, velocity, and altitude have not been fully explored. Axel J. Roenneke presented a tracking control law governing the dynamics of

the re-entry equations expressed in terms of the altitude, velocity, and flight path angle in 1992. And Alberto Cavallo proposed an LQR control scheme for re-entry in 1996. Ping Lu presented a reference trajectory obtained from an SQP (Sequential Quadratic Programming) in 1997. This reference trajectory is the function of energy. However, their analyses concerning the reference trajectory have not been fully developed.

This paper proposes the detailed analyses of reference trajectories for stable re-entry. The reference trajectories are analyzed by calculating the velocity-drag acceleration and velocity-altitude for atmospheric re-entry space vehicle. The longitudinal/lateral control of trajectory are conducted by using a simple nonlinear control law and bank reversals. The result on the azimuth error reveals the importance of lateral trajectory control. In order to reduce the drag acceleration tracking errors at initial and final regimes of the re-entry phase, this paper suggests the fixed bank angle method. Using this method, the drag acceleration tracking error is reduced to about 0.8m/sec^2 at the final regime of the re-entry phase.

2. Mathematical Modeling

2.1 Dynamics of re-entry for space vehicle

The equations of re-entry motion for space vehicles can be described under the following assumptions.

- The earth is assumed to be a rotating sphere.
- The non-thrusting re-entry vehicle is assumed to be a point mass from the vertical plane of the earth.

With these assumptions, the dynamics of re-entry are

$$\begin{aligned}
\dot{R} &= V\sin\gamma \\
\dot{V} &= -D-\frac{\mu\sin\gamma}{R^2} \\
V\dot{\gamma} &= Du+\left(V^2-\frac{\mu}{R}\right)\frac{\cos\gamma}{R} \\
&\quad +2\Omega_E V\cos\phi\sin\psi \\
\dot{\phi} &= \frac{V\cos\gamma\cos\psi}{R} \\
\dot{\theta} &= \frac{V\cos\gamma\sin\psi}{R\cos\phi}
\end{aligned} \tag{1}$$

$$\begin{aligned}
\dot{\psi} &= \frac{L\sin\sigma}{V\cos\gamma}+\frac{V\cos\gamma\sin\psi\tan\phi}{R} \\
&\quad -2\Omega_E(\tan\gamma\cos\psi\cos\phi-\sin\phi) \\
u &= \frac{C_L}{C_D}\cos\sigma
\end{aligned} \tag{2}$$

$$D=\frac{\rho S_{ref}V^2C_D}{2m},\quad L=\frac{\rho S_{ref}V^2C_L}{2m} \tag{3}$$

where R is the radial distance from the earth center to the space vehicle, V is the earth-relative velocity, γ is the flight path angle, D is the drag acceleration, μ is the gravity constant, u is the control variable that is a function of the bank angle, and Ω_E is the angular velocity of the rotation of earth. The latitude and longitude are ϕ and θ, respectively. ψ is the azimuth angle, L is the lift, and σ is the bank angle. $\dot{R}$, $\dot{V}$, and $V\dot{\gamma}$ represent the rate of decent, the progress directional acceleration, and the longitudinal acceleration respectively. C_L and C_D are the lift coefficient and drag coefficient, respectively. ρ is the atmospheric density, S_{ref} is the reference surface area, m is the mass of the space vehicle. An important feature during gliding is that the flight path angle is small compared with ballastic flight. The space vehicle used in this study has a mass of 10020kg and a reference surface area of 79m^2.

2.2 Atmospheric models

Generally, the atmosphere is limited to the height of 120km from the sea level. Atmospheric models can be expressed by the either U.S. standard atmosphere or the exponential atmosphere

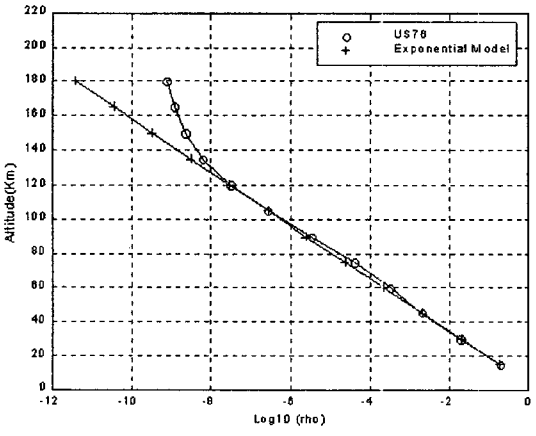

Fig. 1 Comparison of atmosphere model

which are both reasonable approximations. Eq. (4) is the expression of atmospheric density, and Fig. 1 shows the variation of density of the 1976 U.S. standard atmosphere and the exponential atmosphere with respect to the altitude. Eq. (4) is the exponential atmospheric model. Here ρ_0 is the density of the atmosphere at sea level, R_0 is the radius of the earth, and h_s is the scale height.

$$\rho=\rho_0 \exp\left(-\frac{R-R_0}{h_s}\right) \tag{4}$$

2.3 Aerodynamic coefficients

The aerodynamic coefficients are functions of the angle of attack, and the angle of attack is the function of velocity. The angle of attack of a re-entry vehicle should be decided to decrease aerodynamic coefficients as shown in Fig. 2 for the protection of the airframe. To protect the airframe from heating during re-entry, the skin of the space vehicle should be covered with protective heat tiles. Usually, however, these tiles are attached only at the under-side and nose cap of the vehicle, and at the leading edge of the wing to reduce the overall weight. The angle of attack should be designed to remain at 43° for the velocity range of 4300~7400m/s to satisfy the heating rate constraint which is the most dominant constraint during high-speeds flight. For the velocities of less than 4300m/s, the angle of attack decreases. Figure 3 is the variation of aerodynamic coefficients with respect to the velocity.

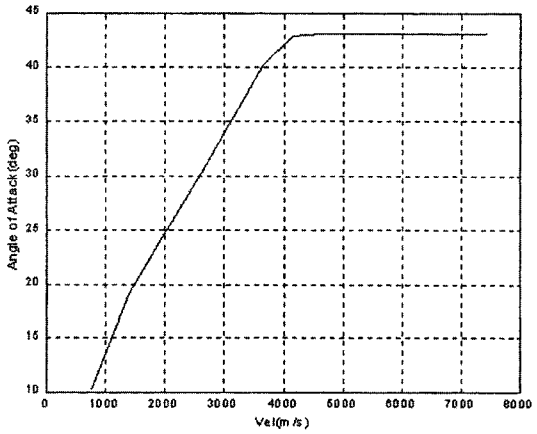

Fig. 2 Angle of attack with respect to velocity

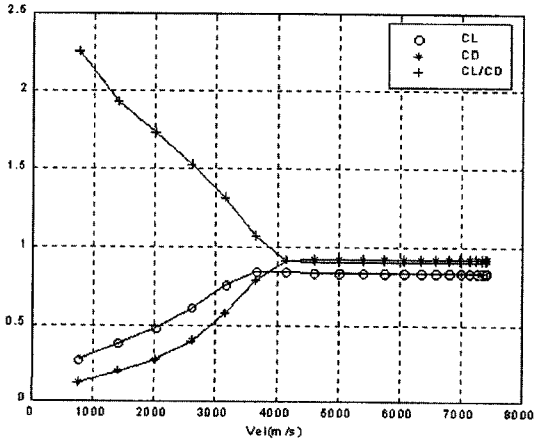

Fig. 3 C_L, C_D, C_L/C_D variation with respect to velocity

3. Generation of Reference Trajectory

The reference drag acceleration is called the reference trajectory. To obtain the reference drag acceleration, it is necessary to develop a profile for the optimal drag acceleration, i.e., the optimal trajectory, by executing optimization of parameters based on the following constraint conditions and performance index.

- Constraint conditions : Heating rate, Load factor, Equilibrium glide, Dynamic pressure, Range error, Dynamic performance
- Performance index : Total heating accumulated in the airframe

3.1 Constraints

All of the constraints, except for the range error, are determined by the design of airframe. These can be expressed as functions of drag acceleration.

1) Heating rate constraint

The heating rate is determined by the performance of the protective heat tiles because it is proportional to the temperature of the outside surface. From the definitions of the heating rate and drag acceleration, the following relation should be satisfied

$$D\leq\frac{C_D S_{ref}\,\dot{q}_{\max}^2}{2m\,C_q^2 V^4} \tag{5}$$

where $\dot{q}_{max}=600{,}000\text{W/m}^2$, and $C_q=1.3\times10^{-4}$.

2) Load factor constraint

The load factor normal to the airframe is determined by the acceleration which the passengers or airframe structure or instruments can bear. This constraint can be expressed as

$$D\leq\frac{n_{max}g_0}{C_L/C_D\cos\alpha+\sin\alpha} \tag{6}$$

where $n_{max}=2.5$ and g_0 is the gravity at the sea level. α is the angle of attack.

3) Equilibrium glide constraint

The equilibrium glide constraint is the limit at which the re-entry vehicle can fly without its nose-down at zero-bank angle. Therefore, if drag acceleration is smaller than the equilibrium glide constraint, the space vehicle stalls. The condition for avoiding the stall is

$$\frac{C_D}{C_L}\left(g-\frac{V^2}{R}\right)\leq D \tag{7}$$

where $g(=\mu/R^2)$ is the Newtonian gravity gradient.

4) Dynamic pressure constraint

The dynamic pressure constraint becomes predominant for the case of high atmospheric density. If the dynamic pressure constraint exceeds the limit, the control surface returns to a neutral condition in spite of the operating control surface. The condition for maximum dynamic pressure provides

$$D\leq\frac{\bar{q}_{max}S_{ref}C_D}{m} \tag{8}$$

where $\bar{q}_{max}=10{,}000\text{N/m}^2$.

5) Range error constraint

The objective of the range error constraint is such that the difference between the actual range s, and the reference range s_{ref}, is zero. The range relation is

$$\dot{s}=V\cos\gamma \tag{9}$$

$$s=\int_{t_0}^{t_f}V\cos\gamma dt=\int_{V_0}^{V_f}\frac{V\cos\gamma}{-D-g\sin\gamma}dV \tag{10}$$

and the constraint has the form of

$$ds=s-s_{ref}\leq\xi(\approx0) \tag{11}$$

6) Dynamic performance constraint

Some re-entry guidance and control designers have designed the permissible flight corridor with the above 5-constraints. In this study, more accurate permissible flight corridor is presented by using the initial condition constraint that is derived by the dynamic performance of the vehicle. Because of the rare atmospheric density at high altitude and the dynamic performance limit due to no-thruster gliding flight, the magnitude of response of drag acceleration is very small despite the manipulation of control surface until about the altitude of 85.5km. Thus the dynamic performance is a stricter constraint than those of the heating rate and equilibrium glide during high-speeds flight. This constraint is composed of bank angles of 0° and 90°.

3.2 Generation of an optimal trajectory

For the generation of the optimal drag acceleration profile, velocities relative to the Earth must be defined first as in Eq. (12). These velocities are divided narrowly at high-speeds because the rate of variation of the velocity is large in these regimes. $iMax$ is the maximum number of break points of the region V.

$$V_i=V_1-(V_1-V_{iMax})\left(\frac{i-1}{iMax-1}\right)^2 \qquad i=1,\ 2,\ \ldots\ iMax \tag{12}$$

The re-entry trajectory is limited by the constraints that determine the magnitude of the drag acceleration. The re-entry corridor is also defined by these conditions. Therefore, the drag acceleration satisfies Eq. (13) which is defined as the minimum drag acceleration D_{lb} and the maximum drag acceleration D_{ub} in each interval i, and is converted by a transformation of Eq. (14). Because D_1 and D_{iMax} satisfy a prescribed flare maneuver, they are fixed values which are obtained from the definition of the drag acceleration.

$$D_{lb}(V_i)\leq D_i\leq D_{ub}(V_i) \qquad i=1,\ 2,\ \ldots\ iMax \tag{13}$$

$$D_i=D_{lb}(V_i)+[D_{ub}(V_i)-D_{lb}(V_i)]\times0.5 \qquad i=2,\ \ldots\ \text{iMax}-1 \tag{14}$$

Optimization is achieved by using SQP (Sequential Quadratic Programming). SQP is a nonlinear programming method and is described in

Table 1 Initial and final conditions for generation of trajectory

Parameter	Value
initial velocity	7400m/s
initial altitude	85.5km
final velocity	760m/s
final altitude	27.5km

detail by R. Fletcher. Approximation at each iteration is solved by taking the Hessian of Lagrangian function using the quasi-newton updating method. In general, this method is also called the constrained nonlinear optimization. Table 1 describes the conditions needed in the generation of reference trajectory.

In this paper, the application of SQP can be explained as the iterative problem for minimizing the total heating on boundary of constraints 1), 2), 3), 4), and 6) until ds becomes less than ξ. With J as the performance index, the optimization problem can be formally stated as

$$\min J=\min \int_{t_0}^{t_f} \sqrt{\rho}\, V^3 dt \qquad (15)$$

$$\text{subject to} \quad ds \leq \xi (\approx 0)$$

Requiring total heating to be a cost function increases the payload. Performance index J which is the function of time, can be approximated as the analytical expression. Analytical performance index J_{analy} is the function of D and V as given by

$$J \approx J_{analy}=F(D,\ V) \qquad (16)$$

Figures 4~6 show the optimal trajectories along the range. Figure 4 shows the case of the specified ranges 2500, 3000, and 3500km respectively. It is evident that optimal trajectories are designed for large drag acceleration in order to shorten the heating-up time of the airframe during flights at speeds exceeding 4594.6m/s. A trajectory with a range of 2500km lies on the upper bound of constraints, which are the heating rate, load factor, and dynamic pressure. Trajectories with in the range between 3000km and 3500km are designed for flights at the lower bound of the equilibrium glide constraint to minimize heating at low-speeds. That is the minimization of atmospheric density and drag acceleration. Figures 5 and 6 depict the trajec-

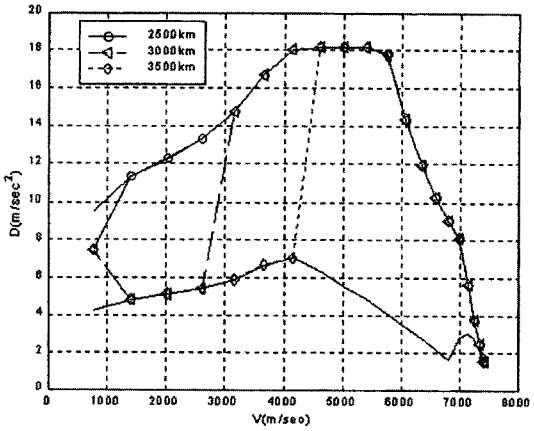

Fig. 4 Optimal drag acceleration along the ranges(Ⅰ)

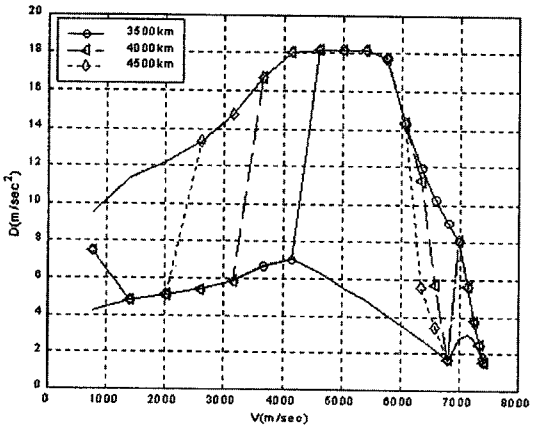

Fig. 5 Optimal drag acceleration along the ranges(Ⅱ)

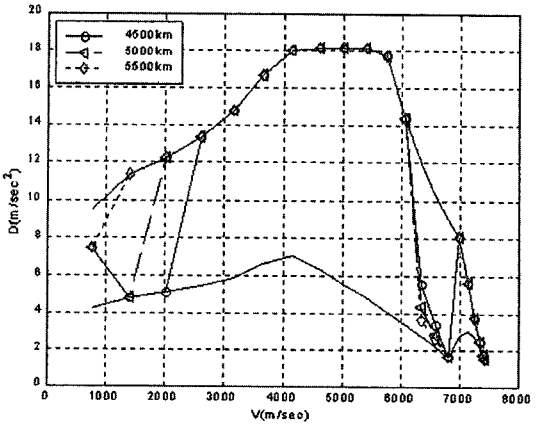

Fig. 6 Optimal drag acceleration along the ranges(Ⅲ)

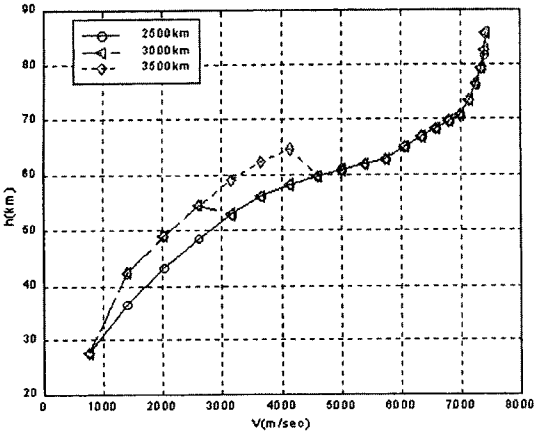

Fig. 7 Altitude variation along the ranges(Ⅰ)

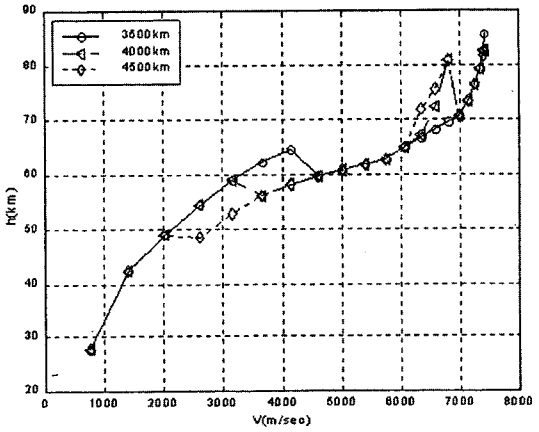

Fig. 8 Altitude variation along the ranges(Ⅱ)

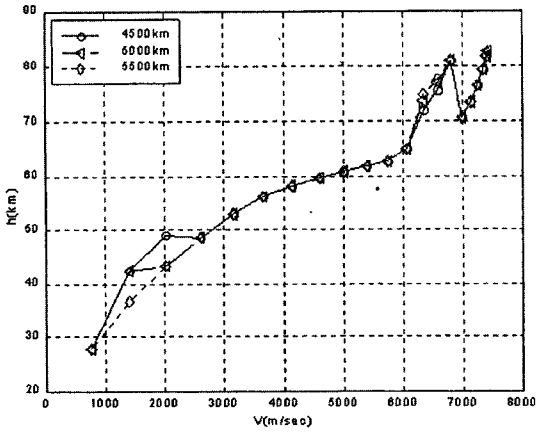

Fig. 9 Altitude variation along the ranges(Ⅲ)

tories above the range of 4000km that have suddenly fallen to the lower bound at the velocity of 7000m/s and then climbed back to the upper bound at around 6800m/s. It is reasonable to reduce heating by reducing atmospheric density, because long range trajectories are at high-speeds for long periods of time.

Table 2 Performance index accordir g to the ranges

Range(km)	J	Range(km)	J
2,500	0.16034	4,500	0.18863
3,000	0.16450	5,000	0.19171
3,500	0.17402	5,500	0.19367
4,000	0.18293		

Figures 7~9 show the variation of the altitude with respect to the velocity corresponding to the optimal trajectories represented in Figs. 4~6. The trajectories over the range of 4000km in Figs. 8 and 9, unlike Fig. 7, descend in order to satisfy a long range at velocities of 7000m/s~6000m/s after a short ascent. This phenomena dilate upon the explanation of the tracing of drag acceleration shown in Figs. 5 and 6. The ascents of altitude at below middle-speeds are shown in Figs. 7~9. These are caused by the sudden descent of optimal drag acceleration into the lower boundary.

Table 2 shows the value of the performance index of the optimal trajectories along the range. The longer the range is, the greater the increase in heating accumulated in the airframe since the space vehicle stays where the heating rate constraint is governed at high-speeds for long periods of time. In Table 2, the value of J is normalized by $g_0(=9.8\text{m/s}^2)$.

3.3 Reference drag acceleration

The performance index acquired from Eq. (16) can not be physically realized. Because the slope of the drag acceleration changes suddenly, it is dangerous to fly on the boundary of constraints with respect to the stability of the re-entry vehicle. To correct such a defect, the regularization parameter ε is introduced to the performance index. With ε, the performance index can be modified as follows :

$$J=\left[\sum_{i=2}^{iMax-1}\Delta J_i+\varepsilon\sum_{i=2}^{iMax-1}\frac{(D_{i+1}-D_i)^2}{V_{i+1}-V_i}\right] \tag{17}$$
$$\begin{cases} D_{lb}(V_i)\le D_i\le D_{ub}(V_i) \\ D_1=D_{initial}(fixed),\ D_{iMax}=D_{final}(fixed) \end{cases}$$

Optimal trajectory acquired through SQP is characterized by the drag acceleration, and expressed as a linear function of the velocity at each break point. In this processing, the 'regularization method' mentioned above is needed to acquire the desired characteristics for the optimal drag profile, and the reference trajectory is represented as D_{ref}. When the iterative calculation of the SQP converges, the reference trajectory is approximated as a third-order polynomial function of the earth-relative velocity in each break point in Eq. (18). It has a continuous form for the integral algorithm as given by

$$D_{ref}(V) = C_1(V - V_i)^3 + C_2(V - V_i)^2 + C_3(V - V_i) + C_4 \quad (18)$$

where C_j $(j=1, 2, 3, 4)$ is the coefficient which change along $i=1, \ldots iMax$.

Figure 10 shows the flow chart for generating D_{ref}. Figures 11 and 12 show the reference drag acceleration and the altitude along the appropriate ranges, and Table 3 represents the performance index when $\varepsilon=0.01$. Figure 13 shows drag acceleration for different values of ε in a fixed range of 4000km, and the performance indices for these cases are presented in Table 4. Despite changing of ε from 0.01 to 0.1, there is not much visible change in the reference trajectory, but the performance index is increased by 152%. Although the performance index ex-

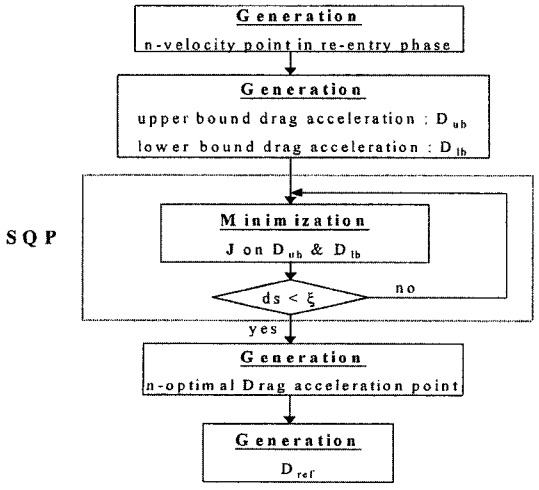

Fig. 10 Flow chart for generation of D_{ref}

Table 3 Performance index for different ranges ($\varepsilon=0.01$)

Range(km)	J
3,500	0.26106
4,000	0.24734
4,500	0.24582

Table 4 Performance index according to ε (range=4000km)

ε	J	ε	J
1	4.38250	0.001	0.20760
0.1	0.62337	0.0001	0.19555
0.01	0.24734	0.00001	0.18418

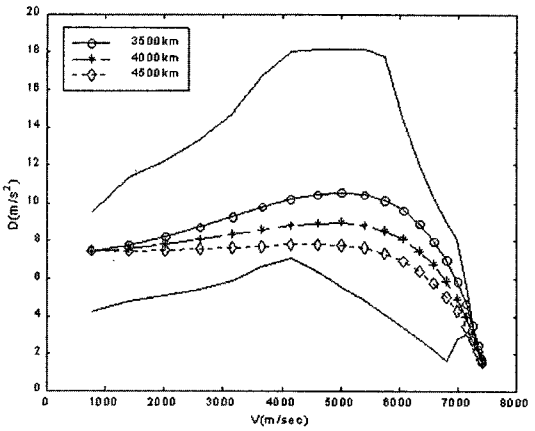

Fig. 11 Reference drag acceleration along the range ($\varepsilon=0.01$)

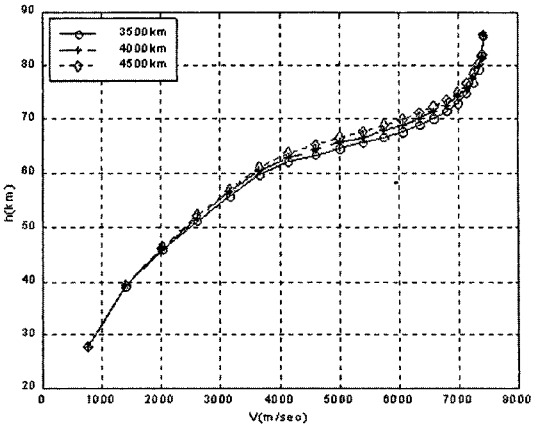

Fig. 12 height variation along the range ($\varepsilon=0.01$)

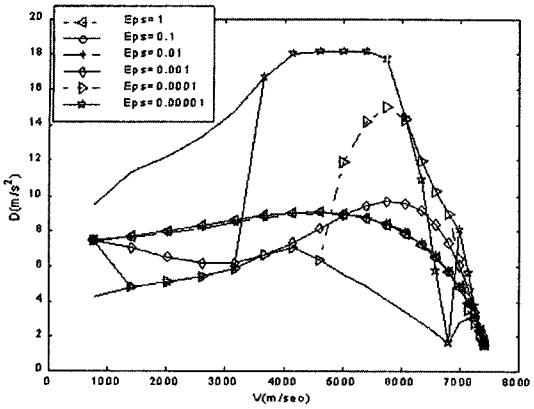

Fig. 13 Reference drag acceleration along epsilon (flight range=4000km)

periences a large increase to 3.38250 when $\varepsilon=1$, the actual performance indices have similar values for visually identical reference trajectories as shown in Fig. 13. Also, compared to the case of $\varepsilon=0$ with the range of 4000km, the performance index with $\varepsilon=0.01$ is increased by 35.21%. This seems to be an acceptable penalty to pay in terms of the performance index in return for much more realistic trajectories.

4. Flight Control System

The flight control system of the re-entry space vehicle consists of a navigation system, a guidance system, and an attitude control system. The role of the navigation system is to transfer the states (position, altitude, velocity, flight path angle etc.) to the guidance systam. The guidance system also consists of longitudinal and lateral guidance. The former has two parts : one generates the reference trajectory which is based on the states, and the other is the trajectory control which is acquired by the attitude angle needed to track the reference trajectory. The role of the latter is to reverse the attitude angle in order to decrease the azimuth error when it exceeds the dead-band limit. The attitude control system used in this paper only controls the bank angle using an aerodynamic control surface, elevon.

4.1 Control of longitudinal trajectory

The space vehicle should be guided to the target

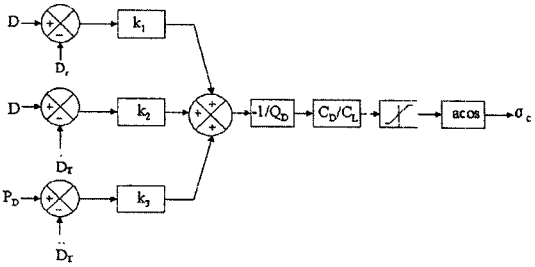

Fig. 14 Block diagram for trajectory control system

states acquired by the generation part of the reference trajectory. These target states should always be maintained inside the permissible flight corridor. These constraints are functions of the velocity and drag acceleration. The velocity decreases monotonously in the case of the no-thrust space vehicle. Accordingly, the representation of the drag acceleration as a function of velocity can guide the states to targets, and can also be expressed in a form in which all of the constraints are within the permissible flight corridor. Thus the target states are the reference states, and they represent the drag acceleration described as a function of velocity. When the optimal drag acceleration is acquired, it is used as the reference drag acceleration in the control system.

Generally, the drag acceleration is determined by the atmospheric density and velocity. In order to increase the drag acceleration for the same velocity, the atmospheric density should be increased. The atmospheric density can be approximated by the 1976 U.S. standard atmosphere. The lower the altitude is, the higher is the atmospheric density. Thus lift should be small to lower the altitude. The bank angle should be controlled for this purpose. From the definition of R, V, D, the relations for these parameters are as follows

$$\begin{aligned}\ddot{R}&=P_R+Q_R u\\ \dot{V}&=P_V+Q_R u\\ \ddot{D}&=P_D+Q_D u\end{aligned} \tag{19}$$

where P_R, Q_R, P_V, Q_V, P_D, Q_D are functions of R, V, γ. Figure 14 is the block diagram that represents a bank angle command (σ_c) for the control of longitudinal trajectory. In Fig. 14, k1, k2 and k3 are the control gains.

4.2 Control of lateral trajectory

Although the space vehicle tracks the reference drag acceleration by the longitudinal trajectory control, lateral range errors orthogonal to the plane of longitudinal trajectory exist. In other words, the roll and yaw motions due to the change of the bank angle increase the tendency of runway bias to one-side. Therefore the control of the lateral trajectory should be considered so thet the no-thrust vehicle will land on the runway. The lateral velocity can be considered separately because it is very slow in comparison with the longitudinal velocity. The azimuth pointing from the current position toward the target point, ψ_{cu-ta}, can be expressed as

$$\psi_{cu-ta}=\frac{\pi}{2}-\tan^{-1}2(\phi_{final}-\phi,\ \theta_{final}-\theta) \quad (20)$$

where ϕ_{final}, θ_{final} are the final latitude and longitude of the vehicle, and $\tan^{-1}2(Y,\ X)$ $(-\pi\leq\tan^{-1}2(Y,\ X)\leq\pi)$ is the four quadrant arc tangent of the real parts of the elements of X and Y.

When the magnitude of the azimuth error $|\psi-\psi_{cu-ta}|$ exceeds a dead-band limit, the control of lateral trajectory results in bank reversals. Mathematically, this is the process for changing the sign of the bank angle. At this time, the dead-band limit should be set to be as small as possible. It is set to be 10° in this study, which is identical to the case of the space shuttle.

Owing to the high atmospheric density at low altitudes, the dynamic performance of the lateral motion as controlled by the bank angle is brisk. Therefore, the tracking error is increased by the bank reversals. Thus, in order to maintain the flight stability at low altitudes, the drop in the tracking performance of the trajectory can be prevented by the fixed bank angle after a sequeuce of bank reversals at some limited velocity.

4.3 Attitude control system

Physical time delays occur when transferring states from the navigation to attitude systems. To represent the physical meaning, the following equation with a first delay mode is inserted into the algorithm.

$$\dot{\sigma}=\frac{1}{T_c}(\sigma_c-\sigma) \quad (21)$$

where T_c is the time constant.

4.4 Fixed bank angle methods

The fixed bank angle methods are applied to two parts(initial/final) of the re-entry phase. One is in the altitude range of 120km~85.5km, the other is in the velocity range of 1200m/s~760m/s. In the former, the bank angle of the region from the altitude of 120km to the initial point of the reference trajectory(D_{ref}) at altitude of 85.5km, is set as a constant because it is impossible to control drag acceleration by changing the bank angle due to a low atmospheric density. This constant value should be selected so that the re-entry vehicle can approach the initial condition of the reference trajectory. In the latter, the bank angle should be fixed to countes the fluctuating lateral motion of the vehicle in the high atmospheric density. The fixed bank angle methods do not always increase the tracking performance. The differences in performance depend on control gains, fixed angle magnitude, and the velocity at which the fixed bank angle is applied. The criteria of a fixed bank angle for the velocity range of 1200m/s~760m/s are as follows

$$\text{if } V<\textit{Velocity at which } \sigma_{fixed} \textit{ is applied}$$
$$\begin{cases}\sigma_c=+(\sigma_{fixed}\ \textit{at low altitude}), & \text{if } \sigma_c>0\\ \sigma_c=-(\sigma_{fixed}\ \textit{at low altitude}), & \text{if } \sigma_c<0\end{cases} \quad (22)$$

4.5 Implementation of Control

Table 5 shows the parameters used in this study.

Table 5 Values of control parameter

Parameter	Value
Range	4,000km
Time constant	0.1sec
Bank angle limit	±90°
Bank angle rate limit	±10°/s
Dead-band limit of azimuth error	±10°
Velocity at which σ_{fixed} is applied	1200m/s
Fixed angle at low altitude	60°
Fixed bank angle between re-entry and initial point of D_{ref}	60°

Figure 15 depicts the drag acceleration histories in the altitude range of 120km~85.5km according to the fixed bank angles. In this study, the bank angle of 60° is verified as the most adequate value. Figure 16 plots the tracking performance of the drag acceleration onto the reference trajectory during both the bank reversals and the non-bank reversals. Figure 17 shows a detailed representation of the circled region in Fig. 16. There are sudden drops of drag acceleration in Figs. 16 and 17. These are caused by a sudden incremental lift at the point $\sigma=0$ during the bank reversal process. The steady-state error in the above figures is caused by neglecting the second derivative of the drag coefficient($d^2C_D/dt^2=0$) and the uncertainty of experimental data. Figure 17 also shows the results of the non-fixed bank angle at a low altitude. In the case of the non-fixed bank angle, tracking performance in the final region is worse than that of the fixed bank angle.

Figure 18 shows the bank angle histories, the difference between the bank reversals and non-bank reversals. The difference becomes noticeable at 400sec.

Figures 19~21 are the flight path angle, earth-relative velocity, and altitude with respect to time, respectively. There is little difference in the bank reversals except for the flight path angle. The sudden variations of the flight path angle are due to the bank reversals, thus the number of the sudden variations are same as that of the bank reversals.

Figure 22 shows the azimuth errors in two cases. There is an azimuth error of 37° in the bank reversals, while the azimuth error of 225° is induced in the case of the non-bank reversals.

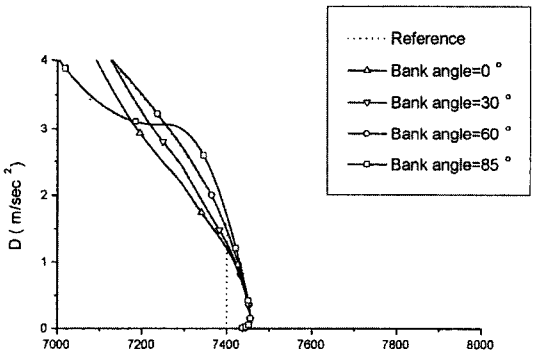

Fig. 15 Drag acceleration histories along the fixed bank angles in 7440m/s~7400m/s

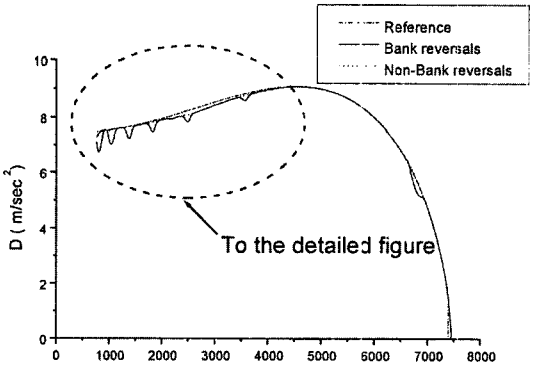

Fig. 16 Drag acceleration histories with respct to velocity

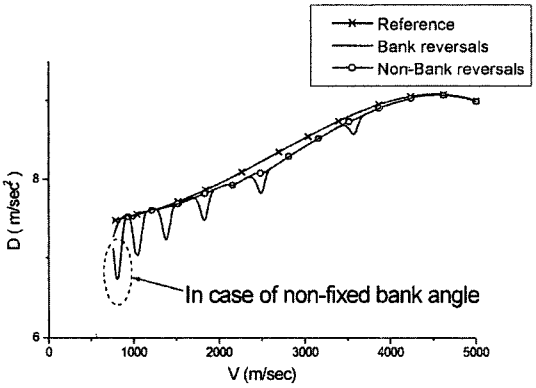

Fig. 17 Detailed representation of drag acceleration histories in low-speed region

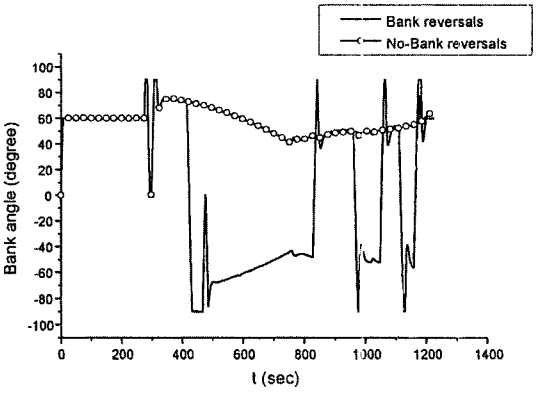

Fig. 18 Bank angle histories with respect to time

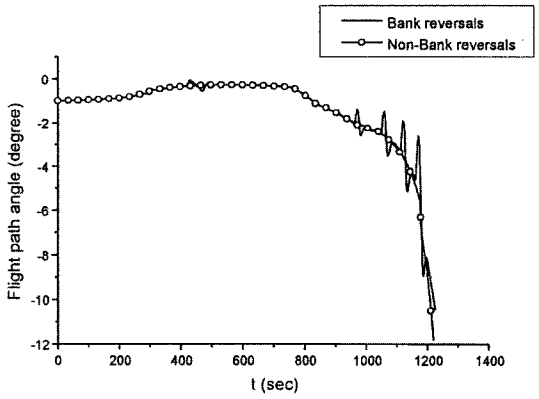

Fig. 19 Flight path angle histories with respect to time

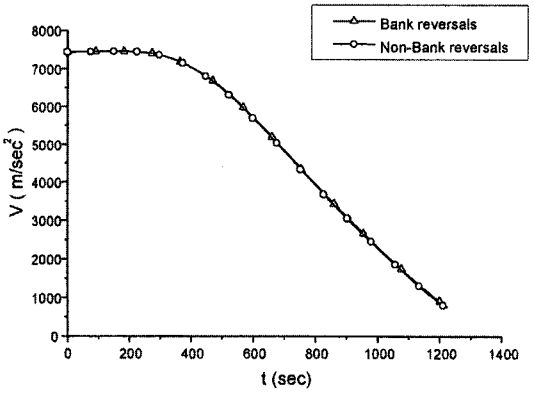

Fig. 20 Earth-relative velocity histories with respect to time

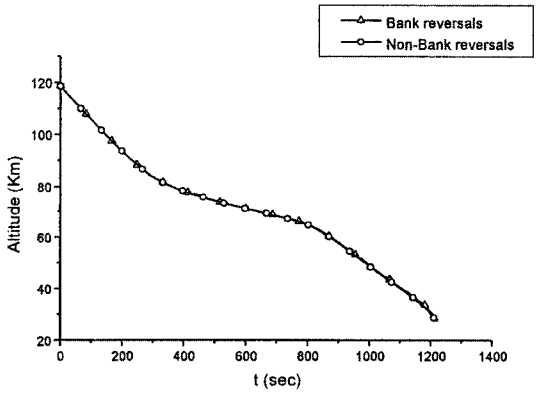

Fig. 21 Altitude histories with respect to time

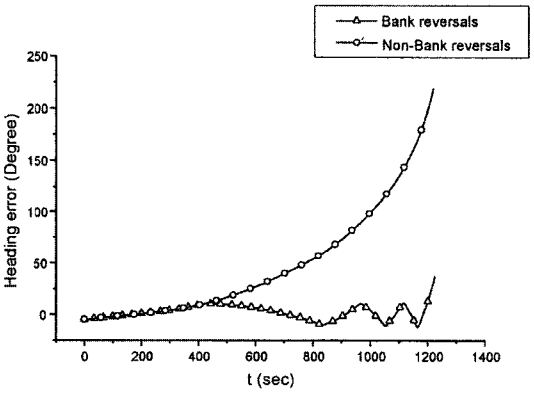

Fig. 22 Azimuth error histories with respect to time

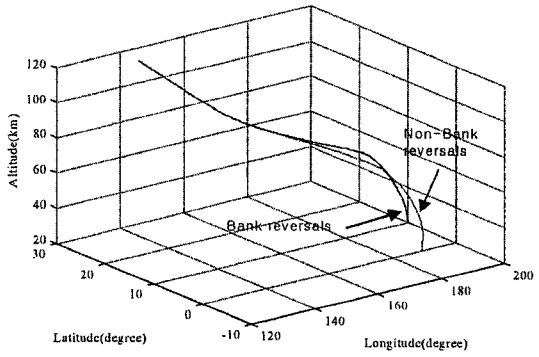

Fig. 23 3-Dimension geometric trajectory

The azimuth error in bank reversals exceeds the dead-band limit, which is caused by the fixed bank angle needed to maintain flight stability and tracking performance at a low altitude. This azimuth error does not have any significant effect on the lateral range error because the altitude is already low, and it can be easily dealt at the TAEM phase. Figure 23 represents the 3-dimensional trajectory for re-entry. It shows the difference between the two cases mentioned due to the bank reversals.

5. Conclusions

It is necessary to design the reference trajectory related to drag acceleration in order to decrease the hypersonic velocity of a space vehicle shortly after atmospheric re-entry. This paper uses the total heating of the airframe as the performance index, and seek to minimize it by applying the SQP method. If the range is designed to be longer, the altitude climbs and suddenly comes down to satisfy the long range at high-speeds.

For realistic reference drag acceleration, the

regularization parameter is introduced into the performance index. Trajectories that are physically realizable can be designed be the suitable scaling of ϵ, and it is verified that the regularization parameter is effective in the scale range from 0.01 to 0.1.

In the control phase, bank reversals and non-bank reversals are simulated using a simple nonlinear controller for longitudinal/later trajectory. The effect of the bank reversals appears in the drag acceleration, the bank angle, the flight path angle, not in the velocity and the altitude. In particular, fixed bank angle methods are shown to reduce drag acceleration error at initial/final parts of the re-entry phase. The steady-state errors in drag accelerations are caused by neglecting the second derivative of the drag coefficient and by the uncertainty in the experimental data. Although the maximum steady-state error is about $0.12 m/s^2$, the proposed method provides a good tracking performance in the permissible flight corridor.

Acknowledgment

This work was supported by the Brain Korea 21 Project.

References

Alberto Cavallo, 1996, "Atmosphere Re-entry Control for Low Lift/Drag Vehicle," *Journal of Guidance, Control, and Dynamics*, Vol. 19, No. 1, pp. 47~53.

Axel J. Roenneke, 1993, "Trajectory Control for a low-Lift Re-Entry Vehicle," *Journal of Guidance, Control, and Dynamics*, Vol. 16, No. 5, pp. 927~933.

Cho S., Cho K. R., 1995, "Nonlinear Adaptive Control for High Angle of Attack Flight," *KSME International Journal*, Vol. 9, No. 2, pp. 147~155.

Fletcher R., 1980, "Practical Methods of Optimization," Vol. 1, *Unconstrained Optimization*, and Vol. 2, *Constrained Optimization*, John Wiley and Sons.

Frank J. Regan and Satya M. Anandakrishnan, 1993, *Dynamics of Atmospheric Re-entry*, AIAA.

Frank P. Incropera and David P. DeWitt, 1985, *Introduction to Heat Transfer*, John Wiley & Sons.

Han, M. C., 1995, "Robust Control of Feedback Linearizable Large-Scale Systems," *KSME International Journal*, Vol. 9, No. 2, pp. 177~186.

Harpold, J. C. and Gavert, D. E., 1979, "Shuttle Entry Guidance," *Journal of Astronautical Sciences*, Vol. 37, No. 3, pp. 239~268.

Lu. P., 1997, "Entry Guidance and Trajectory Control for Reusable Launch Vehicle," *Journal of Guidance, Control, and Dynamics*, Vol. 20, No. 1, pp. 143~149.

Morozov, V. A., 1993, *Regularization Methods for Ill-Posed Problems*, CRC Press Boca Raton, FL, pp. 192~209.

Pouliot, M. R., 1982, CONOP2:A Rapidly Convergent Constrained Trajectory Optimization Program for TRAJEX, *General Dynamics*, Rept. GDCSP- 82-008, Convair Div., San Diego, CA.

Schittowski K., 1985, "NLQPL:A FORTRAN-subroutine Solving Constrained Nonlinear Programming Problems," *Operations Research*, Vol. 5, pp. 485~500.

Slotine J. J. E. and Li Weiping, 1991, *APPLIED NONLINEAR CONTROL*, Prientice Hall.